O_2 Evolution in the Fenton Reaction

Francesco Buda,*[a, c] Bernd Ensing,[a] Michiel C. M. Gribnau,[b] and Evert Jan Baerends*[a]

Abstract: We investigated the mechanism involved in the oxygen production in the Fenton chemistry by means of density functional theory calculations. This study extends previous work in which we proposed that the $Fe^{IV}O^{2+}$ complex is the key active intermediate in the Fenton reaction. Here we provide a consistent picture of the entire reaction cycle by analyzing how the active species, $Fe^{IV}O^{2+}$, can react with hydrogen peroxide to produce O_2 and regenerate the Fe^{2+} catalyst. These results are also relevant in view of the analogies with important enzyme-catalyzed oxidation reactions.

Keywords: density functional calculations · Fenton reaction · ferryl-oxo complex · oxidation

Introduction

The Fenton reagent,[1] a mixture of ferrous ions and hydrogen peroxide in water, has great relevance for the chemical industry in view of its powerful oxidizing properties. Indeed, Fenton reagents are used in the hydroxylation of aromatic substrates (e.g., production of phenol with benzene as a substrate),[2] or for the treatment of contaminated waters containing nonbiodegradable organic compounds.[3] Moreover, the oxidative reactions of the Fenton chemistry show analogies with fundamental processes in biology which are involved in the etiology of diseases.[4] Therefore, an understanding of the microscopic mechanisms of the Fenton chemistry is of fundamental importance and may have an impact on very different fields and applications.

Though the history of the Fenton chemistry extends over more than a century, basic questions about its mechanism and the nature of the active intermediate still remain controversial.[5, 6, 7] There are basically two alternative models which have been proposed in the literature: in the first mechanism, introduced by Haber and Weiss[8] and subsequently modified by Barb et al.,[9] the oxidative intermediate is identified with the free hydroxyl radical formed by the metal-catalyzed decomposition of the hydrogen peroxide; the second mechanism involves the formation of a highly reactive, high-valent iron complex, such as the ferryl-oxo complex first proposed by Bray and Gorin.[10]

Recently, we used density functional theory (DFT) calculations and ab initio molecular dynamics simulations to investigate the initiation step in the Fenton reaction, both in the vacuum[11] and in the presence of the water solvent.[12–14] The main conclusion of this work is that a ferryl-oxo complex can easily be produced in water starting from a primary intermediate with the hydrogen peroxide coordinated to the ferrous ion. The alternative model, in which a free $OH^{\bullet}$ radical, obtained from the hydrogen peroxide dissociation, diffuses into the solvent seems energetically unlikely. Thus, our results strongly support a mechanism in which the Fe^{IV}-oxo complex acts as the key intermediate.

Experimentally, in an excess of H_2O_2 with respect to Fe^{2+} ions, catalytic decomposition of hydrogen peroxide to produce water and O_2 accompanies the oxidation of Fe^{2+} ions [Eq. (1)]:[15]

$$2\,H_2O_2 \rightarrow 2\,H_2O + O_2 \qquad (1)$$

Evidently, in order for FeO^{2+} to be a viable active intermediate, it should also be able to lead to O_2 production in the presence of excess H_2O_2. It is the purpose of this paper to investigate possible reaction mechanisms for the O_2 production with the FeO^{2+} intermediate.

Within the widely accepted hydroxyl radical mechanism, the O_2 production has been explained in the absence of other reagents, for example, an organic substrate, according to the following reaction sequence:

Hydroxyl radical $HO^{\bullet}$ mechanism:

Initiation reaction [Eq. (2)]:

$$Fe^{2+} + H_2O_2 \rightarrow Fe^{3+} + OH^- + HO^{\bullet} \qquad (2)$$

[a] Dr. F. Buda, Prof. E. J. Baerends, Dr. Ir. B. Ensing
Department of Theoretical Chemistry, Vrije Universiteit
De Boelelaan 1083, 1081 HV Amsterdam (The Netherlands)
[b] Dr. M. C. M. Gribnau
Unilever Research Vlaardingen (The Netherlands)
[c] Dr. F. Buda
Leiden Institute of Chemistry, Leiden University
P.O. Box 9502, 2300 RA, Leiden (The Netherlands)

DOI: 10.1002/chem.200204444

O_2 production [Eqs. (3)–(5)]:

$$HO^{\bullet} + H_2O_2 \rightarrow H_2O + HOO^{\bullet} \quad (3)$$

$$HOO^{\bullet} + H_2O_2 \rightarrow O_2 + H_2O + HO^{\bullet} \quad (4)$$

$$HOO^{\bullet} + Fe^{3+} \rightarrow Fe^{2+} + H^+ + O_2 \quad (5)$$

Degradation reaction [Eq. (6)]:

$$HO^{\bullet} + Fe^{2+} \rightarrow Fe^{3+} + OH^- \quad (6)$$

The initiation step [Eq. (2)] produces the active intermediate $HO^{\bullet}$ and the Fe^{3+} ion; Reactions (3)–(5) describe the consumption of H_2O_2 and concomitant evolution of O_2; the third step is a degradation step [Eq. (6)] in which the catalyst is consumed by producing $Fe^{3+}+OH^-$. Reactions (3) and 4 together describe the so-called Haber–Weiss cycle, a chain reaction which consumes the H_2O_2 reagent under O_2 evolution. There is considerable evidence against this "Haber–Weiss cycle" (see the recent review by Koppenol[16]), and it is now considered much more likely that Reaction (5), which regenerates the Fe^{2+} catalyst, is responsible for the O_2 production, although the concentration ratio $[Fe^{3+}] \ll [H_2O_2]$ is not in favor of Reaction (5).

The question we want to address here is how the O_2 production can be explained within a mechanism in which not the $HO^{\bullet}$ but the $Fe^{IV}O^{2+}$ complex is the active species. According to the model initially proposed by Bray and Gorin,[10] the following reaction sequence may describe the catalytic cycle:

Fe^{IV}-oxo complex mechanism:

Initiation reaction [Eq. (7)]:

$$Fe^{2+} + H_2O_2 \rightarrow FeO^{2+} + H_2O \quad (7)$$

O_2 production [Eq. (8)]:

$$FeO^{2+} + H_2O_2 \rightarrow Fe^{2+} + O_2 + H_2O \quad (8)$$

Degradation reaction [Eq. (9)]:

$$FeO^{2+} + Fe^{2+} + H_2O \rightarrow 2Fe^{3+} + 2HO^- \quad (9)$$

The initiation step [Eq. (7)] produces the FeO^{2+} active intermediate; the second step [Eq. (8)] describes the H_2O_2 consumption and concomitant evolution of O_2 as well as the regeneration of the Fe^{2+} catalyst; the third step [Eq. (9)] represents a possible catalyst termination reaction.

A full understanding of the Fenton reaction mechanism must explain not only the initiation step and the nature of the active species, but also the O_2 evolution and the catalyst regeneration. In our previous theoretical work,[11–14] we focused on the formation of the active intermediate (initiation step [Eq. (7)] in the reaction sequence above). In the present paper, we extend our DFT investigation to the O_2 production plus regeneration of the catalyst (Fe^{2+}) in the Fenton reaction, assuming that the Fe^{IV}-oxo complex is the active species formed. Specifically, we focus on Reaction (10) (second step [Eq. (8)] of the reaction sequence above):

$$[(H_2O)_5Fe^{IV}O]^{2+}H_2O_2 \rightarrow [(H_2O)_6Fe^{II}]^{2+} + O_2 \quad (10)$$

We assume implicitly an excess of hydrogen peroxide with respect to Fe^{2+} ions, since oxygen production is actually observed experimentally under such conditions. Therefore, the aim of this work is two-fold: we want to explore the microscopic mechanism behind the oxygen production, and at the same time present evidence for the ferryl-oxo model by providing a consistent picture for the experimentally observed oxygen production in the Fenton reaction. We consider three different routes as a possible first step towards the reaction product (see Scheme 1): i) direct O–O bond formation, ii) hydrogen abstraction, and iii) ligand exchange of hydrogen peroxide with a water in the first coordination shell.

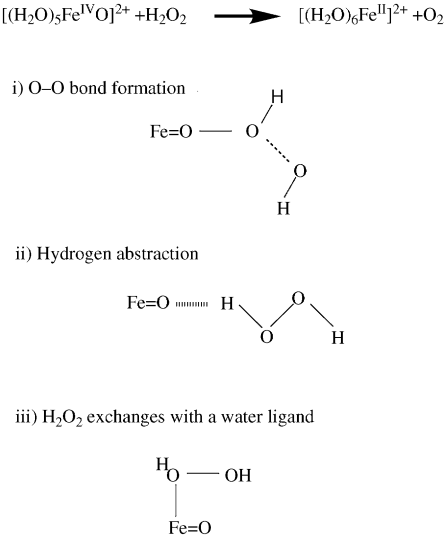

Scheme 1. Mechanisms for O_2 evolution.

Herein, we describe and compare the results obtained for the alternative scenarios considered, and also discuss the implications of these results for the efficiency of the Fenton reaction within the context of the controversy concerning the radical and non-radical mechanisms proposed in the literature.

Methods and Calculations

The density functional theory[17] calculations were performed with the ADF (Amsterdam Density Functional) code.[18] We used the Generalized Gradient Approximation (GGA) in the form proposed by Becke and Perdew[19, 20] (BP) which has been shown to be accurate in reproducing the electronic structure and geometry of the hexaaqua-Fe^{2+} complex.[11] In the ADF code, the electronic orbitals are written in terms of Slater-type orbitals (STO). We use a triple-zeta basis set with one polarization function (this choice corresponds to the basis set IV in the ADF package). The orbital 1s of oxygen and the orbitals up to the 3p of Fe are included as core functions in the calculations.

Frequency calculations have been calculated for all structures appearing in the Figures. They confirm the results of the geometry optimizations and the transition state searches. In particular, the transition states are all

characterized by a single imaginary frequency, and the corresponding mode corresponds to the expected crossing of the barrier maximum. The geometry optimizations have led to proper minima; however, the following comment is in order: in a number of cases there is one extremely low frequency mode (sometimes even below the numerical precision of the calculation, and then either negative or positive). This corresponds in each case to a practically free rotation around a very weak bond between a first coordination sphere ligand and a second coordination sphere ligand. In two cases, the weak bond is a hydrogen bond, namely that depicted in Figure 1a and Figure 3d. In the case of Figure 4a, this concerns a bond between the O of the FeO group and the O of the incoming hydrogen peroxide.

Results

Molecular orbital analysis of the Fe^{IV}-oxo complex: We start this section with a molecular orbital (MO) analysis of the ferryl-oxo complex since this picture will be useful in the interpretation of the reactivity with hydrogen peroxide described in the following. Moreover, we introduce here some of the orbital notation which will be used throughout the paper.

We found that the $[(H_2O)_5Fe^{IV}O]^{2+}$ complex has a high-spin ground state ($S=2$) with an average $Fe-O_{water}$ distance of 2.11 Å, and a short Fe–O distance of 1.63 Å.[11] The Fe–O bonding in this complex can be described in analogy to the bonding situation in triplet dioxygen, as already pointed out in the literature for iron-oxo species in the gas phase.[21]

Indeed the ground state of FeO^{2+} (assuming the FeO bond along the z axis) has a $1\sigma^2 2\sigma^2 1\pi_x^2 1\pi_y^2 \delta_{xy}^1 \delta_{x^2-y^2}^1 2\pi_x^1 2\pi_y^1$ configuration, with four singly occupied orbitals (see Table 1). where O(1s) and Fe 1s–3p are considered as core orbitals and are not included in the orbital count. The triplet state of O_2 shows the same binding block, that is, above the O(2s) orbitals three doubly occupied (σ^2, $1\pi_x^2$, $1\pi_y^2$) bonding orbitals, and two singly occupied antibonding orbitals ($2\pi_x^1$, $2\pi_y^1$). In the case of FeO^{2+}, the $O_{2p}-O_{2p}$ σ and π (anti)bonding is replaced by the $Fe_{3d}-O_{2p}$ σ and π bonding and antibonding. The two electrons that FeO^{2+} has in excess of O_2 enter the up-spin nonbonding $3d\delta$ orbitals. Note that the α spin orbitals are stabilized by a few eV with respect to the corresponding β spin orbitals, as a consequence of the exchange potential.

The MO structure of the $[(H_2O)_5Fe^{IV}O]^{2+}$ complex in Table 2 can be understood from the perturbation of the basic FeO^{2+} pattern of Table 1 by the aqua ligands as follows. We recognize as the 10 lowest levels in Table 2 (the $12a^{\uparrow}-16a^{\downarrow}$ block) the set of H_2O σ lonepair ($2a_1$)-derived spin orbitals. Next, one encounters the up-spin π orbitals of FeO^{2+} (17,18a$^{\uparrow}$) and the $\delta_{xy}^{\uparrow}$. The degeneracy of this orbital with $\delta_{x^2-y^2}^{\uparrow}$ is, however, totally lost, the $\delta_{x^2-y^2}^{\uparrow}$ is strongly destabilized by pushing up by water lonepair orbitals, the antibonding combination ending up as 26a$^{\uparrow}$, 2.7 eV above the $\delta_{xy}^{\uparrow}$ (19a$^{\uparrow}$). The $2\sigma^{\uparrow}$ of FeO^{2+}, with more d_{z^2} character, see Table 1, is destabilized somewhat more

Table 1. One-electron energies and percent composition (in brackets) of the lowest unoccupied and highest occupied molecular orbitals of $Fe^{IV}O^{2+}$ in the $S=2$ ground state.

Orbital	α [eV]	Spin α	Spin β
		unoccupied orbitals	
$2\pi_x^{\downarrow}$, $2\pi_y^{\downarrow}$ (antib.)	−22.1		p_x, p_y (56) − d_{xz}, d_{yz} (42)
$3\sigma^{\downarrow}$ (antib.)	−22.2		d_{z^2} (61) − p_z (25)
$3\sigma^{\uparrow}$(antib.)	−23.3	p_z (48) − d_{z^2} (37)	
$\delta_{xy}^{\downarrow}$, $\delta_{x^2-y^2}^{\downarrow}$ (non-bond.)	−23.5		d_{xy}, $d_{x^2-y^2}$
		occupied orbitals	
$2\pi_x^{\uparrow}$, $\pi_y^{\uparrow}$ (antib.)	−24.5	p_x, p_y (67) − d_{xz}, d_{yz} (32)	
$1\pi_x^{\downarrow}$, $1\pi_y^{\downarrow}$ (bond.)	−25.3		d_{xz}, d_{yz} (58)+p_x, p_y (41)
$2\sigma^{\downarrow}$(bond.)	−27.0		p_z (63)+d_{z^2} (28)
$\delta_{xy}^{\uparrow}$, $\delta_{x^2-y^2}^{\uparrow}$ (non-bond.)	−27.3	d_{xy}, $d_{x^2-y^2}$	
$1\pi_x^{\uparrow}$, $1\pi_y^{\uparrow}$ (bond.)	−27.8	d_{xz}, d_{yz} (67)+p_x, p_y (32)	
$2\sigma^{\uparrow}$ (bond.)	−28.3	d_{z^2} (53)+p_z (39)	
$1\sigma^{\downarrow}$	−40.0		2s (95)
$1\sigma^{\uparrow}$	−40.9	2s (97)	

Table 2. One-electron energies and percentage composition (in brackets) of the lowest unoccupied and highest occupied molecular orbitals of $[(H_2O)_5Fe^{IV}O]^{2+}$ in the $S=2$ ground state in terms of the FeO^{2+} and $(H_2O)_5$ fragments. The $2a_1$ and $1b_2$ orbitals correspond to the HOMO − 1 σ lonepair and HOMO π lonepair of the waters, respectively.

Orbital	ε [eV]	Spin α	Spin β
		unoccupied orbitals	
29a$^{\downarrow}$	−12.61		3σ (83) − $2a_1$ (9)
28a$^{\downarrow}$	−13.61		$\delta_{x^2-y^2}$ (81) − $1b_2$ (10)
27a$^{\downarrow}$	−13.64		$2\pi_y$ (96)
26a$^{\downarrow}$	−13.72		$2\pi_x$ (94)
29a$^{\uparrow}$	−14.07	3σ (81) − $2a_1$ (10) − $1b_2$ (5)	
25a$^{\downarrow}$	−14.74		δ_{xy} (90) − $1b_2$ (8)
		occupied orbitals	
		FeO^{2+} levels	
28a$^{\uparrow}$	−16.02	$2\pi_y$ (95) − $1b_2$ (2)	
27a$^{\uparrow}$	−16.06	$2\pi_x$ (93) − $1b_2$ (5)	
26a$^{\uparrow}$	−16.32	$\delta_{x^2-y^2}$ (51) − $1b_2$ (34) − $2a_1$(11)	
24a$^{\downarrow}$	−16.78		$1\pi_y$ (53) − $1b_2$ (40)
23*a*$^{\downarrow}$	−17.09		$1\pi_x$ (53) − $1b_2$ (41)
		H_2O-1b_2 levels	
25*a*$^{\uparrow}$	−17.33	$1b_2$ (72) − δ_{xy} (25)	
24*a*$^{\uparrow}$	−17.39	$1b_2$ (86) − $1\pi_y$ (4)	
23*a*$^{\uparrow}$	−17.49	$1b_2$ (90)+$1\pi_x$ (4)+$2\pi_x$ (4)	
22*a*$^{\downarrow}$	−17.51		$1b_2$ (92)+$1\pi_y$ (7)
21*a*$^{\downarrow}$	−17.78		$1b_2$(64)+$1\pi_x$ (28)
20*a*$^{\downarrow}$	−17.81		$1b_2$(72)+$1\pi_x$ (14)
19*a*$^{\downarrow}$	−17.87		$1b_2$(79)+δ_{xy}(5)
22*a*$^{\uparrow}$	−17.85	$1b_2$ (90)+$1\pi_y$ (4)	
21*a*$^{\uparrow}$	−18.13	$1b_2$(45)+$2a_1$ (37)+$\delta_{x^2-y^2}$ (13)	
18a$^{\downarrow}$	−18.27		$1b_2$ (56)+$1\pi_y$ (37)
		FeO^{2+} levels	
17a$^{\downarrow}$	−18.38		2σ (78) − $2a_1$ (13)
20a$^{\uparrow}$	−18.91	2σ (61) − $2a_1$ (32)	
19a$^{\uparrow}$	−19.02	δ_{xy} (71)+$1b_2$ (24)	
18a$^{\uparrow}$	−19.58	$1\pi_x$ (90)+$1b_2$ (3)	
17a$^{\uparrow}$	−19.65	$1\pi_y$ (77)+$1b_2$ (11)+$2a_1$ (6)	
		H_2O-2a_1 levels	
16a$^{\downarrow}$	−20.17		$2a_1$(88)
15a$^{\downarrow}$	−20.33		$2a_1$(70)+2σ (9)+$\delta_{x^2-y^2}$ (7)
16a$^{\uparrow}$	−20.40	$2a_1$(76)+$1\pi_y$ (13)	
14a$^{\downarrow}$	−20.54		$2a_1$ (88)
15a$^{\uparrow}$	−20.70	$2a_1$ (86)+$1\pi_x$ (2)	
13a$^{\downarrow}$	−20.82		$2a_1$ (76)+2σ (9)+$\delta_{x^2-y^2}$ (6)
14a$^{\uparrow}$	−20.97	$2a_1$ (44)+2σ (26)+$\delta_{x^2-y^2}$(13)+$1b_2$ (8)	
13a$^{\uparrow}$	−21.33	$2a_1$ (63)+$\delta_{x^2-y^2}$ (14)+2σ (12)	
12a$^{\downarrow}$	−21.56		$2a_1$ (83)+3σ (4)
12a$^{\uparrow}$	−21.86	$2a_1$ (76)+$\delta_{x^2-y^2}$ (8)+3σ (7)	

by the axial water $2a_1$ than the down-spin $2\sigma^{\downarrow}$ with considerably less d_{z^2} character. The gap between the $2\sigma^{\uparrow}$, $2\sigma^{\downarrow}$ pair ($20a^{\uparrow}$, $17a^{\downarrow}$) is reduced to 0.53 eV in the aqua complex. The 10 H_2O $1b_2$ lonepair spin orbitals are inserted in between the $2\sigma^{\downarrow}$ and $1\pi_x^{\downarrow}$, $1\pi_y^{\downarrow}$ of FeO^{2+}. They push $\delta_{xy}^{\uparrow}$ down, so it ends up just below $2\sigma^{\uparrow}$ while in FeO^{2+} it was 1 eV above $2\sigma^{\uparrow}$. The lowest unoccupied α-spin orbital is the FeO^{2+} $3\sigma^{\uparrow}$ antibonding orbital ($d_{z^2} - 2p_z$), pushed up by H_2O lonepairs ($29a^{\uparrow}$). This orbital is particularly relevant for the reactivity with hydrogen peroxide as we will discuss in the following.

Thermodynamic stability of the reaction: Before discussing the possible microscopic reaction mechanisms, we first establish whether the Reaction (10) is endothermic or exothermic. A geometry optimization of the reactants complex on the left-hand side of Reaction (10) (complex **1** throughout the paper) shows that the hydrogen peroxide forms a strong hydrogen bond with one of the water ligands (Figure 1a). The complexation energy, that is the energy gain involved in the formation of this hydrogen-bonding interaction, is 24.7 kcal mol^{-1}, thus much higher than the typical hydrogen bond strength of 4 kcal mol^{-1}. Also the O···O distance of 2.53 Å is much shorter than the 2.88 Å found for the typical hydrogen bond in a water dimer by means of the same functional. This result is analogous to that previously found for the interaction between a pentaaqua-Fe^{2+} complex with a water in the second coordination shell.[11] An analysis of the different energy contributions has shown that this bond has a much higher electrostatic contribution in comparison to the H bond found, for example, in a water dimer. We notice also that, in the complex **1** (Figure 1a), an electronic charge of 0.16 e (according to a Mulliken population analysis) is transferred from the HOOH molecule to the Fe-oxo complex. The dihedral angle of the HOOH is 102° (compared to ≈110° for HOOH in the vacuum). We have chosen the energy of the optimized reactants complex **1** to be equal to zero for the following comparisons.

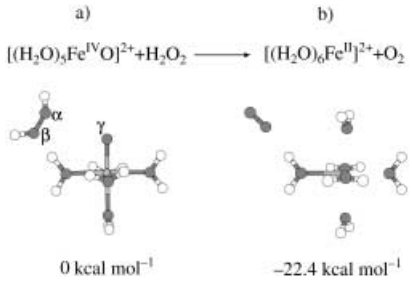

Figure 1. Optimized geometries of a) the reactants complex, the ferryl-oxo complex plus hydrogen peroxide in the second coordination shell, and b) of the final products, the hexaaqua-ferrous complex plus O_2.

In Figure 1b, we show the optimized geometry of the product on the right-hand side of Equation (10) (complex **2** throughout the paper). The dioxygen molecule is in its triplet ground state ($S = 1$) and forms a hydrogen bond with one water ligand of the ferrous complex. In this case, the O···O hydrogen bond length is 2.86 Å and the complexation energy is only ≈4 kcal mol^{-1}, thus corresponding to a typical hydrogen bond. The hexaaqua-Fe^{2+} complex is in the high-spin ($S = 2$) ground state (for a detailed description of the electronic structure of this complex see ref.[11]). The total energy of the product in Figure 1b is 22.4 kcal mol^{-1} lower than the reactants complex, therefore the overall reaction is highly exothermic according to our DFT-BP calculations.

Note that the total spin changes in Reaction (10): in fact the Fe complex is in the $S = 2$ state on both sides; however, the ground state of O_2 is a triplet at variance from H_2O_2 which has $S = 0$. The spin state is important for the determination of the correct energetics of the reaction because, for example, the triplet state of O_2 is experimentally ≈22.5 kcal mol^{-1} lower than the singlet. The DFT calculation yields an excitation energy of 26 kcal mol^{-1}, which is a typical accuracy for an excitation energy with a GGA functional. There is no danger that singlet oxygen inadvertently plays a role in the calculations caused by an erroneous low energy of this state.

Direct O–O bond formation mechanism: We now investigate the various reaction mechanisms of Scheme 1, starting with i), direct O–O bond formation. Starting from the local minimum of Figure 1a, we follow the reaction path defined by the distance between the oxygen on the iron complex O^{γ} and the oxygen O^{α} of H_2O_2 not involved in the hydrogen bond. The energy profile along this reaction coordinate is shown in Figure 2. The energy at each reaction coordinate value is

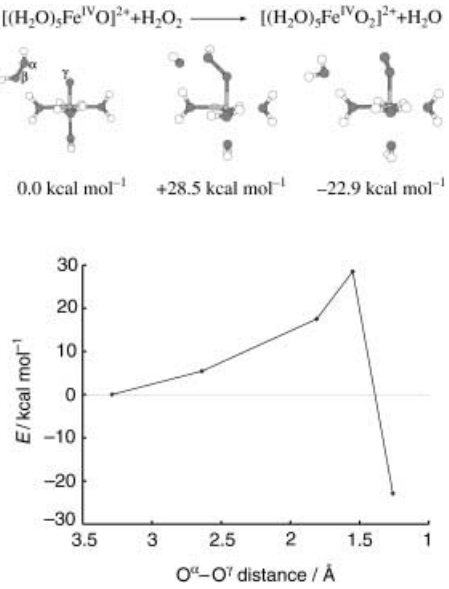

Figure 2. O–O bond formation mechanism: energy as a function of the distance between the oxygen O^{γ} of the ferryl-oxo complex and the O^{α} of H_2O_2 not involved in the hydrogen bonding. We also show the configurations of the reactants complex (taken as zero of energy), transition state, and product with their relative energies.

obtained by fixing the O^{α}–O^{γ} distance and optimizing all the other coordinates. A transition state (TS) is found for an O–O distance of 1.56 Å with an activation energy of 28.5 kcal mol^{-1}. Note, however, that this activation energy would be only ≈4 kcal mol^{-1} with respect to the free reactants (see complexation energy in the previous section). The TS complex (Figure 3a) can be described as a pentaaqua-Fe^{III}-

hydroperoxo complex plus a hydroxyl radical. Therefore, we have a concomitant cleavage of the hydrogen peroxide $O^{\alpha}-O^{\beta}$ bond and the formation of a new $O^{\alpha}-O^{\gamma}$ bond which gives rise to an OOH ligand. The activation energy is, however, quite high since we lose energy in going from the strong Fe–O bond to the weaker Fe–OOH bond. This can also be seen from the increased Fe–O bond length (from 1.63 to 1.83 Å at the TS) which is, in turn, related to the population of the antibonding 3σ orbital of FeO^{2+}.

Figure 3 shows a few snapshots describing the geometry optimization starting from a configuration very close to the TS (Figure 3a) up to the final product $[(H_2O)_5Fe^{IV}O_2]^{2+} + H_2O$ with dioxygen coordinated to iron and a water molecule in a second coordination shell position (Figure 3d). We observe that the OH radical abstracts a hydrogen from one water ligand to form a new water molecule and an OH ligand coordinated to iron (Figure 3b). This process is very similar to that observed in the first step of the Fe^{IV}-oxo complex formation starting from H_2O_2 coordinated to Fe^{II} and leading to a tetraaqua-Fe^{IV}-dihydroxo compound.[11] However, the $[(H_2O)_4Fe^{IV}(OH)(OOH)]^{2+}$ complex is not stable in the presence of the noncoordinated water because a proton is spontaneously transferred from the OOH ligand to the OH ligand through this water molecule (Figure 3c, d). This formation of coordinated O_2 from coordinated OOH by transfer of the H via an intermediate H_2O to a coordinated OH, transforming it into coordinated H_2O, is completely analogous to the formation of the ferryl-oxo from the dihydroxo complex by transfer of H from one OH ligand, via an intermediate water molecule, to the other OH.[11] After full geometry relaxation the total binding energy of the product (Figure 3d) (complex **3** throughout the paper) is 22.9 kcal mol^{-1} lower than the initial complex **1**.

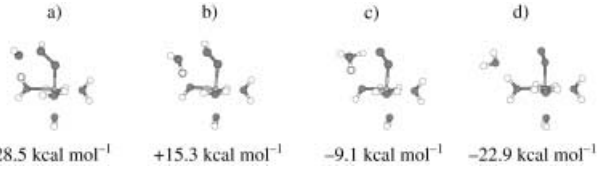

Figure 3. O–O bond formation mechanism: A few configurations and energies are shown relative to the optimized reactants complex along the geometry optimization starting from the transition state up to the formation of the final complex with O_2 coordinated to the pentaaqua-iron complex.

The reaction described in Figure 2 and 3 proceeds with constant total spin $S=2$. We notice that the energy of $[(H_2O)_5Fe^{IV}O_2]^{2+}\cdot H_2O$ (Figure 3d), -22.9 kcal mol^{-1}, is very close to that obtained for $[(H_2O)_6Fe^{II}]^{2+}\cdot O_2$ (Figure 1b), -22.4 kcal mol^{-1}. Therefore, the exchange of the dioxygen ligand with a water molecule in the second coordination shell is energetically possible. This step leads to the final product with the regeneration of the catalyst and O_2 production. However, it should be pointed out that complex **2** has a total spin $S=3$, the O_2 being in the triplet state. Therefore, we have to assume that some spin-flip process (induced by, e.g., spin–orbit interaction) changes the total spin in the complex **3** from $S=2$ to $S=3$, followed by the departure of the O_2 molecule. The calculated energy of complex **3** in the $S=3$ total spin state is -22.1 kcal mol^{-1}, thus the spin-flip does not imply a significant energetic penalty. The additional α-spin density is localized on the O_2 ligand, which goes from a singlet to a triplet configuration (see also Table 3). Table 3 shows the optimized geometry of complex **3** with the dioxygen ligand in the $S=2$ and $S=3$ spin state. The main effect of the spin polarization on the O_2 ligand is to significantly elongate the bond with the iron center.[22] Indeed a MO analysis shows that in going from $S=2$ to $S=3$, an electron moves from a β-spin MO characterized by a π bonding between one of the $1\pi_g$ O_2 orbitals and the Fe δ_{yz} orbital, to an α-spin MO (unoccupied in the $S=2$ state) with a π antibonding character between the other $1\pi_g$ O_2 orbital and the Fe δ_{xy} orbital. We have estimated the bonding energy of the O_2 ligand with the pentaaqua-Fe complex to be ≈ 6 kcal mol^{-1} in the triplet configuration, and ≈ 32 kcal mol^{-1} in the singlet configuration. For comparison, the bonding energy of a sixth water ligand to $[Fe(H_2O)_5]^{2+}$ is 24.5 kcal mol^{-1}.[11] Thus, the dioxygen ligand in the triplet state can leave the complex **3** and exchange with a water molecule more easily.

Table 3. Geometry of the complex $[Fe(H_2O)_5O_2]^{2+}\cdot H_2O$ optimized with the BP functional and with total spin $S=2$ and 3, respectively. The energy is relative to the reactants complex $[Fe(H_2O)_5O]^{2+}\cdot H_2O_2$.

$[Fe(H_2O)_5O_2]^{2+}\cdot H_2O$	$S=2$	$S=3$
E [kcal mol^{-1}]	–22.9	–22.1
Fe–O dist [Å] (eq. W)	2.13	2.13
Fe–O dist [Å] (ax. W)	2.18	2.20
Fe–O dist [Å] (O_2)	1.94	2.23
O–O dist [Å] (O_2)	1.26	1.25
Fe-O-O angle [°]	130	156
charge [e], spin $\left(\frac{\hbar}{2}\right)$ on O_2	–0.06, 0.03	0.04, 1.91

Hydrogen abstraction mechanism: We now consider a different reaction path in which the hydrogen peroxide approaches the Fe-oxo complex along the FeO direction. We find a local minimum, shown in Figure 4a (complex **4**), which is only 5.3 kcal mol^{-1} higher in energy compared to the local minimum described above (Figure 1a). The complexation energy is thus 19.3 kcal mol^{-1} in this case. However, the interaction between the hydrogen peroxide and the Fe^{IV}-oxo complex has a very different nature in this configuration: first of all we mention that, in spite of the large $O^{\alpha}-O^{\gamma}$ distance of 2.63 Å, a considerable electronic charge (about 0.5 e) is transferred from the hydrogen peroxide to the oxo-complex. As a consequence of this charge transfer, the geometry of the hydrogen peroxide becomes almost *trans*-planar with a dihedral angle of 194°. This configuration is 3 kcal mol^{-1} higher than the optimized geometry of H_2O_2 in vacuum, which has a torsional angle of 110°. Thus, the torsion costs relatively little energy, but the π* HOMO of H_2O_2 rises in energy by about 1 eV. A *trans*-planar geometry is the ground state of the isolated $H_2O_2^+$ ion. An inspection of the molecular orbitals of complex **4** shows that the electronic charge transfer occurs from the antibonding π* HOMO of H_2O_2 to the

antibonding α-spin LUMO ($29a^{\uparrow}$ in Table 2, mostly (81%) 3σ of FeO^{2+}) of the Fe^{IV}-oxo complex (the 3σ of FeO^{2+} has much O_{2p_z} character). The charge transfer is only between α-spin orbitals, the FeO^{2+} $3\sigma^{\downarrow}$ ($29a^{\downarrow}$ in the complex, see Table 2) being at too high energy. So that the total spin density on the ferryl-oxo complex increases and also the H_2O_2 becomes spin polarized, but with a net spin density of opposite sign. Figure 4b, c gives the α-spin HOMO and LUMO, respectively, of the complex shown in Figure 4a. This illustrates the $3d_{z^2} - 2p_z$ antibonding character of FeO^{2+} LUMO 3σ. The HOMO clearly shows that, when the H_2O_2 approaches the Fe^{IV}-oxo complex along the Fe–O direction, a bonding overlap arises between the HOMO of H_2O_2 and the lowest unoccupied α-spin state (3σ) on the ferryl complex. The LUMO is just the antibonding combination of these two orbitals.

A few structural changes are noticeable which occur as a consequence of this charge transfer: the Fe–O distance is slightly elongated (1.68 vs 1.63 Å) as a consequence of the population of the 3σ antibonding orbital and the $O^{\alpha}-O^{\beta}$ bond of the peroxide is shortened (1.42 vs 1.48 Å) because of a smaller antibonding charge. In this local minimum, the H^{α} of H_2O_2 is at 2.63 Åfrom the O^{γ} of the iron complex, that is at the same distance as the O^{α}.

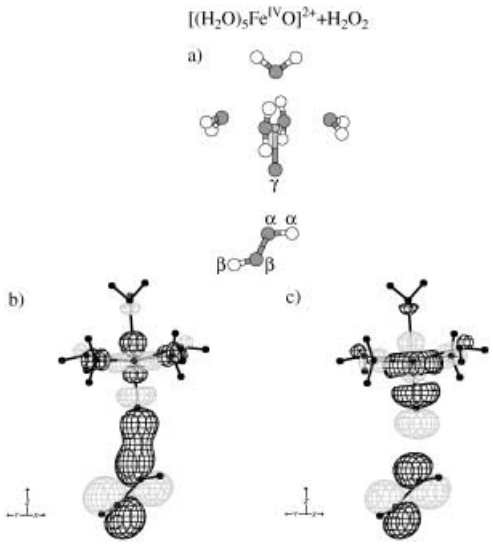

Figure 4. a) Local minimum with the H_2O_2 approaching the ferryl complex along the Fe–O direction. b) and c) The α-spin HOMO and LUMO of this complex, respectively. The partial population of the 3σ orbital of the ferryl-oxo complex is evident.

We follow now the reaction path obtained by decreasing the $O^{\gamma}-H^{\alpha}$ distance. The energy profile for the hydrogen abstraction reaction [Eq. (11)] is shown in Figure 5 together with a few configurations along the path:

$$[(H_2O)_5Fe^{IV}O]^{2+} + HOOH \rightarrow [(H_2O)_5Fe^{III}OH]^{2+} + OOH^{\cdot} \quad (11)$$

$$(S=2)+(S=0) \rightarrow (S=5/2) + (S=-\tfrac{1}{2})$$

The energy of the transition state configuration, which occurs for a $O^{\gamma}-H^{\alpha}$ distance of 1.52 Å(Figure 5, second configuration), is 6.9 kcal mol^{-1} with respect to the same zero of energy as in Figure 1a, and only 1.6 kcal mol^{-1} higher than the local minimum described above (Figure 5, first configuration). Along this path, the remaining charge (and spin) density on the α-spin π* orbital orthogonal to the plane of $OOH^{\cdot}$ is progressively transferred to the 3σ orbital. In Equation (11) we have also explicitly indicated the total spin of the particles involved to illustrate that the number of unpaired spins can change during the reaction although the total spin is conserved. Indeed, the ground state of isolated complex $[(H_2O)_5Fe^{III}OH]^{2+}$ has a total spin $S=2.5$ with five unpaired electrons.

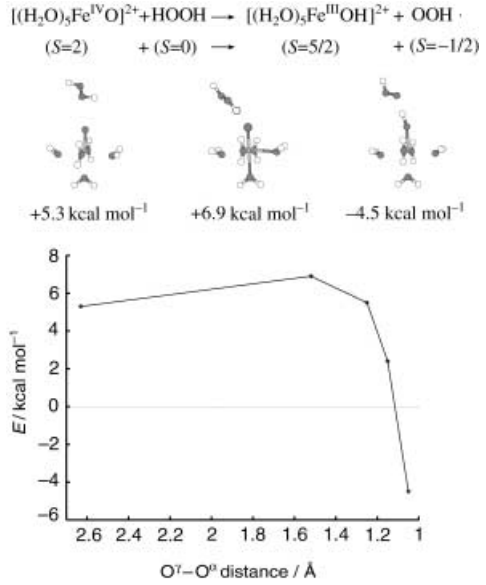

Figure 5. First step of the hydrogen abstraction mechanism: energy profile along the $O^{\gamma}-H^{\alpha}$ distance for the H-abstraction reaction.

In order to obtain the final product of the reaction with the production of dioxygen, a second abstraction step is needed [Eq. (12)].

$$[(H_2O)_5Fe^{III}OH]^{2+} + OOH^{\cdot} \rightarrow [(H_2O)_6Fe^{II}]^{2+} + O_2 \quad (12)$$

$$(S=2.5) + (S=\tfrac{1}{2}) \rightarrow (S=2) + (S=1)$$

Therefore, the $OOH^{\cdot}$ radical has to rotate so that the H comes close to the oxygen of the OH ligand. We find that this "reorientation process" costs ≈9.5 kcal mol^{-1}, and that the H is easily abstracted by the OH ligand from $OOH^{\cdot}$ to form a water ligand plus O_2 in the triplet state (Figure 6). Reaction (12) is also exothermic by ≈18 kcal mol^{-1}.

It would be interesting to perform first-principles molecular dynamics simulation to see how the reorientation process of the $OOH^{\cdot}$ radical can occur at room temperature in the presence of the water solvent. We expect that the estimated energy of 9.5 kcal mol^{-1} in the vacuum may change significantly as a result of the interaction of the radical with the water molecules in the solvent. Moreover, another scenario may be conceived in which the $OOH^{\cdot}$ radical propagates into the solvent initiating a chain reaction, as described in the

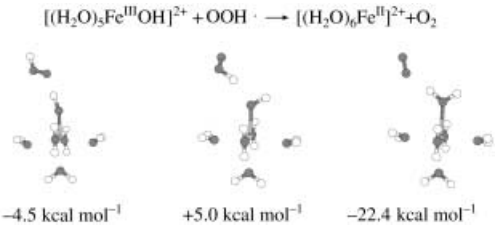

Figure 6. Second step in the hydrogen-abstraction mechanism: a hydrogen is abstracted from the OOH· radical to form the hexaaqua-Fe^{II} complex and O_2.

Haber and Weiss radical mechanism. This will be the subject of further investigations.

Based on the present results in the vacuum, we can conclude that Mechanism ii) of Scheme 1 is feasible, and it appears to be more likely than Mechanism i) because it involves much lower energy barriers.

Reaction paths starting from hydrogen peroxide coordinated to the ferryl-oxo complex: We now consider the third scenario (iii) in Scheme 1) in which the hydrogen peroxide first exchanges with a water in the first coordination shell of iron and then the dioxygen is produced [Eq. (13)].

$$[(H_2O)_4(H_2O_2)Fe^{IV}O]^{2+} \rightarrow [(H_2O)_5Fe^{IV}O_2]^{2+} \quad (13)$$

The binding energy of a water molecule in $[(H_2O)_5Fe^{IV}O]^{2+}$ and of the hydrogen peroxide ligand in $[(H_2O)_4(H_2O_2)$-$Fe^{IV}O]^{2+}$ is approximately the same according to our calculations. Therefore, this ligand exchange has no energetic penalty.

O–O bond formation: The energy of the complex $[(H_2O)_4(H_2O_2)Fe^{IV}O]^{2+}$ with total spin $S=2$ is taken as a reference energy in the following. The optimized geometry of this complex shows a $Fe-O^{\alpha}$ bond length with H_2O_2 of 2.37 Å, thus quite elongated if compared with the same bond length in the pentaaqua-Fe^{II}-H_2O_2 complex (2.21 Å). Moreover, the hydrogen peroxide is oriented so as to form a strong hydrogen bond between the O^{β} and the H of a water ligand ($O^{\beta}-H^{\beta}$ bond length = 1.70 Å) similarly to the ground state geometry of pentaaqua-Fe^{II}-H_2O_2.[11]

We now consider a reaction path in which the O^{β} of H_2O_2 forms the bond with the O^{γ} ligand (Figure 7). If we rotate the hydrogen peroxide along the $Fe-O^{\alpha}$ axis, we find a local minimum at an energy of $+2.3$ kcal mol^{-1} (see first configuration in Figure 7), which corresponds to the energy needed to break the $O^{\beta}-H^{\beta}$ hydrogen bond present in the global minimum. The relevant distances in this configuration are $Fe-O^{\alpha}$ 2.16, $O^{\alpha}-O^{\beta}$ 1.466, and $O^{\beta}-O^{\gamma}$ 2.95 Å.

By elongating the $O^{\alpha}-O^{\beta}$ bond of the hydrogen peroxide, a transition state is found at a distance of 1.91 Å (Figure 7) with an activation energy of 29.8 kcal mol^{-1}. Along this reaction path the $O^{\alpha}-O^{\beta}$ bond cleavage is followed by the formation of an OOH ligand and the reaction is exothermic by 9.6 kcal mol^{-1} as illustrated in Figure 7 [Eq. (14)].

$$[(H_2O)_4Fe^{IV}(H_2O_2)O]^{2+} \rightarrow [(H_2O)_4Fe^{IV}(OOH)(OH)]^{2+} \quad (14)$$

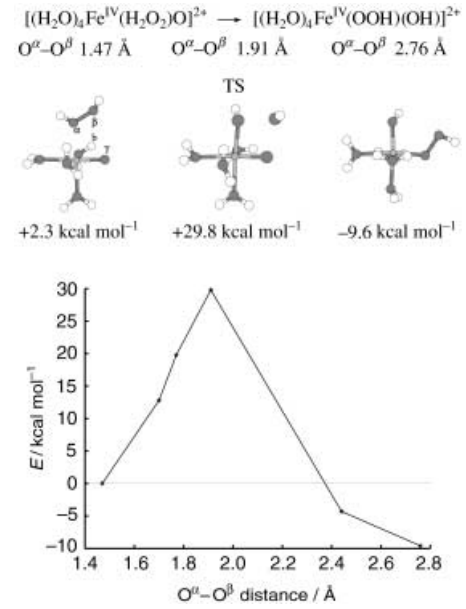

Figure 7. Energy profile for the O–O bond-formation mechanism starting from a coordinated H_2O_2 as a function of the distance between the oxygen atoms of the peroxide. The configurations and relative energies of the initial complex, the TS, and the product are shown. The O–O bond cleavage is followed by the formation of a OOH ligand. The zero of energy corresponds to the optimized geometry (not shown) in which the hydrogen peroxide is oriented so as to form a strong hydrogen bond between the O^{β} and the H of a water ligand (H^{b} in the figure).

The energy barrier in this process is very close to that found for the O–O bond formation mechanism already described above for the direct mechanism starting from a hydrogen peroxide which was not in the first but in the second coordination shell of iron. In the section describing the direct O–O bond formation mechanism, we also observed that the complex $[(H_2O)_4Fe^{IV}(OOH)(OH)]^{2+}$ in the presence of a noncoordinated water molecule spontaneously decays to the more stable complex $[(H_2O)_5Fe^{IV}O_2]^{2+}$ (Figure 3). This second reaction step provides a further energy gain of 13.7 kcal mol^{-1}. Overall, the Reaction (13) is exothermic by 23.3 kcal mol^{-1}. In conclusion, the O–O bond formation mechanism is not significantly modified by having the H_2O_2 in the first coordination shell of Fe instead of in the second coordination shell because this mechanism is still not likely owing to the high energy barrier of 29.8 kcal mol^{-1}.

Hydrogen abstraction: We have also considered the mechanism in which the H abstraction occurs from the coordinated H_2O_2. Figure 8 shows a few selected configurations along this path together with the energy as a function of the $O^{\gamma}-H^{\beta}$ distance.

The increase in energy in the first part is related to the breaking of the internal hydrogen bond between the peroxide and one water ligand (as described in the previous subsection). A plateau is observed for a distance of ≈ 2 Å when the bonding of the peroxide ligand with the iron becomes stronger and the peroxide becomes almost planar. When we further reduce the $O^{\gamma}-H^{\beta}$ distance, the $Fe-O^{\alpha}$ bond weakens considerably and finally when the H is abstracted and the

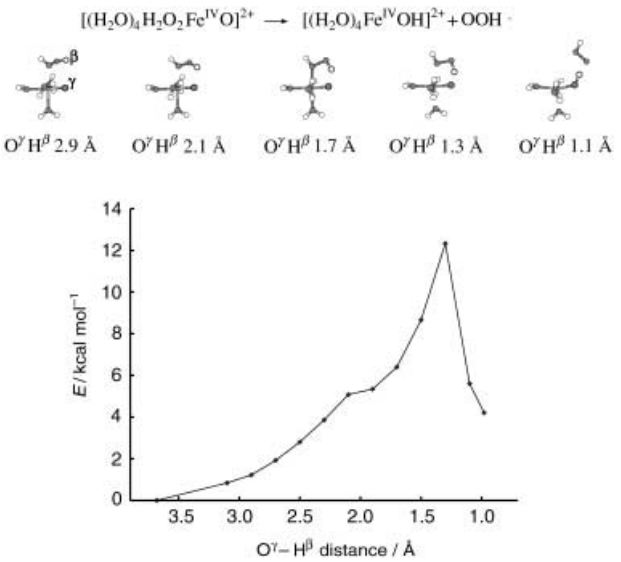

Figure 8. Energy profile for the H-abstraction mechanism starting from a coordinated H_2O_2. We also show a few configurations along this path which illustrate the reaction.

OH ligand is formed, the OOH radical moves out of the first coordination shell. The energy barrier in this reaction path is ≈ 12 kcal mol^{-1} and the energy of the final configuration is actually higher than the initial complex by ≈ 4 kcal mol^{-1}. However, it should be noted that, in the presence of the water solvent, coordination of a water molecule to the empty site would considerably lower the energy. In conclusion, the H abstraction mechanism starting from a coordinated peroxide has an energy barrier somewhat higher than that in the case of the H_2O_2 in the second coordination shell. Therefore, the coordination of the peroxide as a first step does not make this route for the O_2 evolution more feasible.

Conclusions

We have analyzed the possible alternative mechanisms for the oxygen evolution in the Fenton reaction by means of a DFT approach. This study assumes a high concentration of hydrogen peroxide and the formation of a ferryl-oxo complex as the key active intermediate. Indeed, we have recently shown by DFT-based Car–Parrinello Molecular Dynamics that a ferryl-oxo complex can easily be produced by the Fenton reagents in water.[12, 13]

Our results show that the oxygen production, which is observed experimentally in the Fenton reaction, can easily be understood in the presence of the ferryl-oxo complex and therefore does not constitute evidence for $OH^{\cdot}$ radicals as intermediates. This provides further support to the model which identifies the ferryl-oxo species as the active oxidizing intermediate in Fenton chemistry.

The hydrogen-abstraction mechanism should be the dominant mechanism for the production of dioxygen molecules in the Fenton cycle. The reaction would thus proceed in two successive H-abstraction steps (Figures 5 and 6) which are both exothermic and involve quite low activation energies. The overall reaction is exothermic by 22.4 kcal mol^{-1} according to our DFT-BP calculations.

The alternative O–O bond-formation mechanism produces the final product in a single step when starting from a second coordination shell H_2O_2, or in two steps from a directly coordinated H_2O_2 (Figure 7); however, in both cases, it involves a much higher transition-state energy.

We should also point out that in the first step of the H-abstraction mechanism, an $OOH^{\cdot}$ radical is produced which, in the presence of the water solvent, might propagate through a radical chain reaction. Therefore the present results point to the possibility that a mixture of radical and nonradical reactions occur in the Fenton chemistry. Our calculations suggest that the active Fe-Oxo intermediate is formed according to a nonradical reaction as in the Bray–Gorin proposal, whereas the O_2 production, under regeneration of the Fe^{2+} catalyst, proceeds with a radical as intermediate. This opens the possibility that characteristics of radical reactions may also be observed.

Finally, within the ferryl-oxo model in high hydrogen peroxide concentrations, the O_2 production acts as competitive reaction to the oxidation of substrate, as it would do in the Haber–Weiss radical mechanism. In fact, part of the hydrogen peroxide will be consumed in O_2 production and will fail to enter an oxidation process, that is, to participate in an initiation step which produces the active ferryl-oxo species.

Acknowledgements

Support from the Netherlands' Priority Programme for Materials Research (Computational Materials Science section) is gratefully acknowledged. Computing budgets for the calculations performed at the Stichting Academisch Rekencentrum Amsterdam (SARA) have been made available by the foundation Nationale Computerfaciliteiten (NCF) of the Netherlands' Foundation for Scientific Research (NWO) and by the Vrije Universiteit.

[1] H. J. H. Fenton, *J. Chem. Soc.* **1894**, *65*, 899–910.
[2] J. P. Hage, A. Llobet, D. T. Sawyer, *Bioorg. Med. Chem.* **1995**, *3*, 1383–1388.
[3] a) S. H. Bossmann, E. Oliveros, S. Göb, S. Siegwart, E. P. Dahlen, L. Payawan, Jr., M. Straub, M. Wörner, A. M. Braun, *J. Phys. Chem. A* **1998**, *102*, 5542–5550; b) E. Oliveros, O. Legrini, A. M. Braun, M. Hohl, T. Müller, *Water Sci. Technol.* **1997**, *35*, 223–230; c) E. Oliveros, O. Legrini, M. Hohl, T. Müller, A. M. Braun, *Chem. Eng. Proc.* **1997**, *36*, 397–405.
[4] B. Halliwell, J. M. C. Gutteridge, *Biochem. J.* **1984**, *219*, 1–14.
[5] For a review, see, for example, P. Wardman, L. P. Candeias, *Radiat. Res.* **1996**, *145*, 523–531.
[6] a) C. Walling, *Acc. Chem. Res.* **1998**, *31*, 155–157; b) D. T. Sawyer, *Coordin. Chem. Rev.* **1997**, *165*, 297–313; c) D. T. Sawyer, A. Sobkowiak, T. Matsushita, *Acc. Chem. Res.* **1996**, *29*, 409–416.
[7] M. L. Kremer, *J. Inorg. Biochem.* **2000**, *78*, 255–257.
[8] F. Haber, J. Weiss, *Proc. R. Soc. London* **1934**, *A147*, 332–351.
[9] W. G. Barb, J. H. Baxendale, P. George, K. R. Hargrave, *Trans. Faraday Soc.* **1951**, *47*, 462–500.
[10] W. C. Bray, M. H. Gorin, *J. Am. Chem. Soc.* **1932**, *54*, 2124–2125.
[11] F. Buda, B. Ensing, M. C. M. Gribnau, E. J. Baerends, *Chem. Eur. J.* **2001**, *7*, 2775–2783.
[12] B. Ensing, F. Buda, P. Blöchl, E. J. Baerends, *Angew. Chem.* **2001**, *113*, 2977–2979; *Angew. Chem. Int. Ed.* **2001**, *40*, 2893–2895.
[13] B. Ensing, F. Buda, P. E. Blöchl, E. J. Baerends, *Phys. Chem. Chem. Phys.* **2002**, *4*, 3619–3627.

[14] B. Ensing, E. J. Baerends, *J. Phys. Chem. A* **2002**, *106*, 7902 – 7910.
[15] M. L. Kremer, *Phys. Chem. Chem. Phys.* **1999**, *1*, 3595 – 3605.
[16] W. H. Koppenol, *Redox Rep.* **2002**, *6*, 229.
[17] See, for example, R. M. Dreizler, E. K. U. Gross, *Density Functional Theory*, *An approach to the Quantum Many-Body problem*, Springer, Berlin, **1990**.
[18] a) E. J. Baerends, D. E. Ellis, P. Ros, *Chem. Phys.* **1973**, *2*, 41; b) P. M. Boerrigter, G. te Velde, E. J. Baerends, *Int. J. Quantum Chem.* **1988**, *33*, 87; c) C. Fonseca Guerra, J. G. Snijders, G. te Velde, E. J. Baerends, *Theor. Chem. Acc.* **1998**, *99*, 391.
[19] A. D. Becke, *Phys. Rev. A* **1988**, *38*, 3098.
[20] J. P. Perdew, *Phys. Rev. B* **1986**, *33*, 8822.
[21] See, for example, D. Schröder, H. Schwarz, S. Shaik, in *Metal-Oxo and Metal-Peroxo Species in Catalytic Oxidations*, *Vol. 97* (Ed.: B. Meunier), Structure and Bonding Series, Springer, Berlin, **2000**, p. 91.
[22] N. Lehnert, R. Y. N. Ho, L. Que, E. I. Solomon, *J. Am. Chem. Soc.* **2001**, *123* 12802–12816.

Received: September 23, 2002
Revised: March 17, 2003 [F4444]